We are IntechOpen,
the world's leading publisher of
Open Access books
Built by scientists, for scientists

4,800
Open access books available

122,000
International authors and editors

135M
Downloads

Our authors are among the

154
Countries delivered to

TOP 1%
most cited scientists

12.2%
Contributors from top 500 universities

BOOK CITATION INDEX
CLARIVATE ANALYTICS
INDEXED

WEB OF SCIENCE™

Selection of our books indexed in the Book Citation Index
in Web of Science™ Core Collection (BKCI)

Interested in publishing with us?
Contact book.department@intechopen.com

Numbers displayed above are based on latest data collected.
For more information visit www.intechopen.com

Specific Absorption Rate Analysis of Heterogeneous Head Models with EEG Electrodes/Leads at 7T MRI

Leonardo M. Angelone[1,2] and Giorgio Bonmassar[2]
*[1]Division of Physics, Office of Science and Engineering Laboratories,
Center for Devices and Radiological Health, U.S. Food and Drug Administration,
Silver Spring, MD
[2]Athinoula A. Martinos Center for Biomedical Imaging, Department of Radiology,
Massachusetts General Hospital, Harvard Medical School, Charlestown, MA
USA*

1. Introduction

In this chapter we explore the use of anatomically accurate head models for radio frequency (RF) dosimetry and design of electroencephalography (EEG) electrode and leads. The study is conducted at 300 MHz, which is the frequency used to elicit the proton-based Magnetic Resonance Imaging (MRI) signal at 7 Tesla (7T). The use of electrically heterogeneous vs. homogeneous numerical models is explored in terms of investigation of antenna-effect for EEG leads. While the results in the homogeneous model can be validated with direct measurements in phantoms, the experimental validation of numerical simulations with electrically heterogeneous head models would require the use of a multi-structure physical phantom, much more cumbersome and expensive to build. This study aimed to evaluate whether the use of a more complex heterogeneous head model would provide additional information when looking at energy absorbed by a human head wearing EEG electrodes/leads and exposed to a 300 MHz RF field.

MRI-based high-resolution homogeneous and heterogeneous head models were implemented for this study. The electromagnetic (EM) interactions between EEG electrodes/leads on the human head and the incident RF field used to elicit the MRI signal were investigated in terms of electromagnetic field, induced currents in the leads, and specific absorption rate (SAR) in a human head. Both perfectly conductive and resistive EEG leads were studied.

Non-significant differences in whole-head SAR (i.e. less than 5%) and a 30% difference in peak-10g-averaged SAR values were observed with the homogeneous vs. heterogeneous models. The difference for peak-1g-averaged SAR estimated with the homogeneous vs. heterogeneous model was up to 100%. The presence of an insulating layer between EEG electrode and skin resulted in a change of 10% of peak-10g-averaged SAR and 280% for peak 1g-averaged SAR. Results of this study suggest that a homogeneous model could be used to estimate the changes on whole-head and 10g-averaged SAR due to the antenna effect of EEG leads at 7 T MRI. Precise modeling of the electrically conductive interface between electrode and head surface is also fundamental.

Simultaneous EEG and MRI/fMRI recordings are frequently performed in clinical research as they provide fundamental information on the physiological and hemodynamic activity of the brain [Allen 2000, Benar 2003, Comi 2005, Kobayashi 2005, Liebenthal 2003, Matsuda 2002, Mirsattari 2004, Mulert 2005, Purdon 2009]. While clinical application for this technology (e.g. epilepsy) are mainly limited to MRI fields up to 1.5 T [Stern 2006], the possibility of increased spatial resolution and signal to noise ratio for brain structural and functional information drives an increasing number of research groups toward the use of high field MRI, namely 3T [Goldman 2000, Iannetti 2005, Purdon 2009, Scarff 2004] and even 7T [Mullinger 2008, Vasios 2006].

EEG recordings at high-field MRI present several technological challenges, including signal and safety issues. The EEG electrodes/leads can affect the MRI signal [Bonmassar 2001], and the MRI can add noise into the EEG signal [Allen 2000, Lemieux 1997]. The safety issues present are intrinsic to high-field MRI [Ibrahim 2007] as well as due to interaction between static, gradient and RF field with EEG electrodes and leads on the human head [Schenk 2000, Shellock 2011].

Safety issues for simultaneous EEG and high-field MRI recordings are typically categorized as: force and torque on device due to static and spatial gradient fields [Schenk 2000], peripheral nerve stimulation due to gradient-switching [Shellock 2011], and potential issues due to induced currents and related adverse thermal effects associated with energy dissipation inside the head [IEC 2002, FDA 2003].Because of the low magnetic permeability of the human body [Polk 1986], RF heating from magnetic energy dissipated inside the human head is typically disregarded and only the electric component of the incident field is considered when calculating RF heating. The electric energy fed into the RF coil of the MRI systems is partly radiated into the empty space and partly dissipated with the EEG leads and the head. If the energy dissipated inside the head is not properly balanced by the thermoregulatory system, potential adverse thermal effects can occur [Adair 1986]. The quantity used to quantify the amount of power dissipated in the human body is the SAR, measured in W/kg [NCRP 1981].

A full evaluation of RF-induced heating requires the calculation of electric field in each point of the volume of interest. The electric coupling can be analyzed in terms of both a) Faraday-induced non-conservative coupling and b) conservative capacitive coupling:

$$\vec{E} = -j\omega\vec{A} - \nabla V \tag{1}$$

Faraday's induced currents ("eddy currents"), represented by the non-conservative term of eq. (1) $j\omega\vec{A}$, are generated by coupling between the MRI gradient and/or RF field and conductive loops within EEG leads, inside the human head, and/or between EEG leads and human head [Dempsey 2001]. Capacitive coupling - represented by the conservative term of eq. (1) ∇V, occurs when the dimensions of the load (i.e., head with leads) are comparable with the incident wavelength, and the time-varying electric component is "picked up" by the load, acting as scattering antennas [Armenean 2004, Balanis 2005, Dempsey 2001, Yeung 2002]. Hence, there is a difference of potential (∇V in eq. 1) due to charge accumulation that contributes to the conservative component of the electric field.

For MRI fields up to 1.5 T the EM wavelength (e.g., 4.7m in empty space at 64 MHz/1.5T) is much longer than dimensions of the head and the capacitive coupling can be disregarded

("quasi-static approximation") [Bottomley 1978]. Consequently, previous studies evaluating RF heating for EEG leads and MRI systems up to 1.5T have mainly focused on faraday-induced eddy currents [Lemieux 1997]. Based on these studies, some solutions have been proposed to overcome the issue of the induced currents along EEG leads, such as twisted pair configuration [Godlman 2002], or the use of current-limiting resistors [Lemieux 1997].

At high field MRI (3 T or higher) however, this approximation is no longer valid (e.g., RF wavelength at 300 MHz/7T in empty space is 1m) and a full-wave characterization of the incident RF field [Ibrahim 2007] is necessary. The full-wave model requires the analysis of the complete Maxwell equations; given the complexity of the geometries considered, numerical solutions have been implemented [Collins 2005, Gandhi 1999, Jin 1997, Kainz 2003, Trakic 2007, Van der Berg 2007]. Among the different algorithms used, the Finite Difference Time Domain [Kunz 1993, Taflove 2005] is often the method of choice.

The "antenna-effect" defines the physical phenomenon for which a conductive lead immersed in an EM field scatters the incident field, becoming a transmitting-antenna [Balanis 2005]. This mechanism creates two different issues: 1) a mismatch of conductivity at the interface between a lead and the skin, with charge accumulation ("capacitive" effect) and enhancement of electric field in the area underneath the electrode [Guy 1975]; 2) a perturbation of the EM field compared to the one generated by the RF coil only, with related changes of SAR in the head.

The currents induced along the EEG leads in an RF field depend on the geometry of the leads, the characteristics of the incident EM field, and the material properties of the lead. The efficiency of the leads as antennas, hence their effect into the incident EM field, is higher for lead dimensions comparable with the wavelength of the incident field. Given the typical length of EEG leads (~50-100 cm) the EM fields generated by rapid gradient switching have wavelengths too long to generate a significant antenna behavior for the EEG leads [Dempsey 2001]. Conversely, the antenna effect of the leads will be significant at the RF frequencies used for imaging. The RF current induced in the leads depend on the relative position of the leads with respect to the incident RF field, being maximal with leads parallel to the RF field and null with the leads perpendicular to the RF field [Balanis 2005].

Given the geometrical complexity of the problem considered, computational EM can help to further understand the interaction between variably-resistive EEG leads and the human body. Whole-body averaged, partial body, and whole-head averaged SAR [IEC 2002, FDA 2003] are the values of reference used in the MRI systems to control the maximum RF transmitted power allowed during an MRI examination. A spatial resolution of 2×2×2.5mm^3 to model the human head is considered accurate when evaluating whole-head SAR in MRI [Collins 2003]. However, in the specific case of a human head with conductive leads during MRI, the interactions between leads and the RF-field are expected to generate local peaks of electric field and SAR near the electrodes [Guy 1975]. In this case, the use of the whole-head SAR as an exclusive dosimetric parameter for safety profile is inaccurate and the estimation of local 1g- or 10g-averaged SAR is more appropriate [Angelone 2010, Nitz 2005]. In this study, the hypothesis that 2×2×2.5mm^3 is sufficient for SAR computation was rejected, and a MRI-based head model with 1×1×1mm^3 isotropic spatial resolution was implemented [Angelone 2008, Makris 2008]. A similar model has been used to study the effect of purely metallic EEG leads [Angelone 2004], to evaluate the use of high resistive leads with numerical simulations on a homogeneous model [MRI 2006], and to evaluate the effect of EEG electrodes/leads in the human head exposed to RF sources of mobile-phone [Angelone

2010]. In this chapter we investigate the effect of using electrically heterogeneous vs. homogeneous human head models.

2. Methods

Numerical head model: Anatomical segmentation and classification at radio-frequency by electrical properties. MRI data - One healthy 37-year-old, right-handed adult male volunteer participated in this study. Informed consent was obtained in accordance with Massachusetts General Hospital policies. High-resolution anatomical MRI data were acquired with a quadrature birdcage transmit/receive head coil on a 1.5 T scanner (General Electric, Milwaukee, WI). Data were collected with a T1-weighted 3D-SPGR sequence (TR/TE = 24/8 ms) with 124 slices, 1.3 mm thick (matrix size 256×192, FOV 256 mm). The volume data was resampled to isotropic voxels with dimensions of 1x1x1 mm³. Segmentation was then applied to this dataset volume.
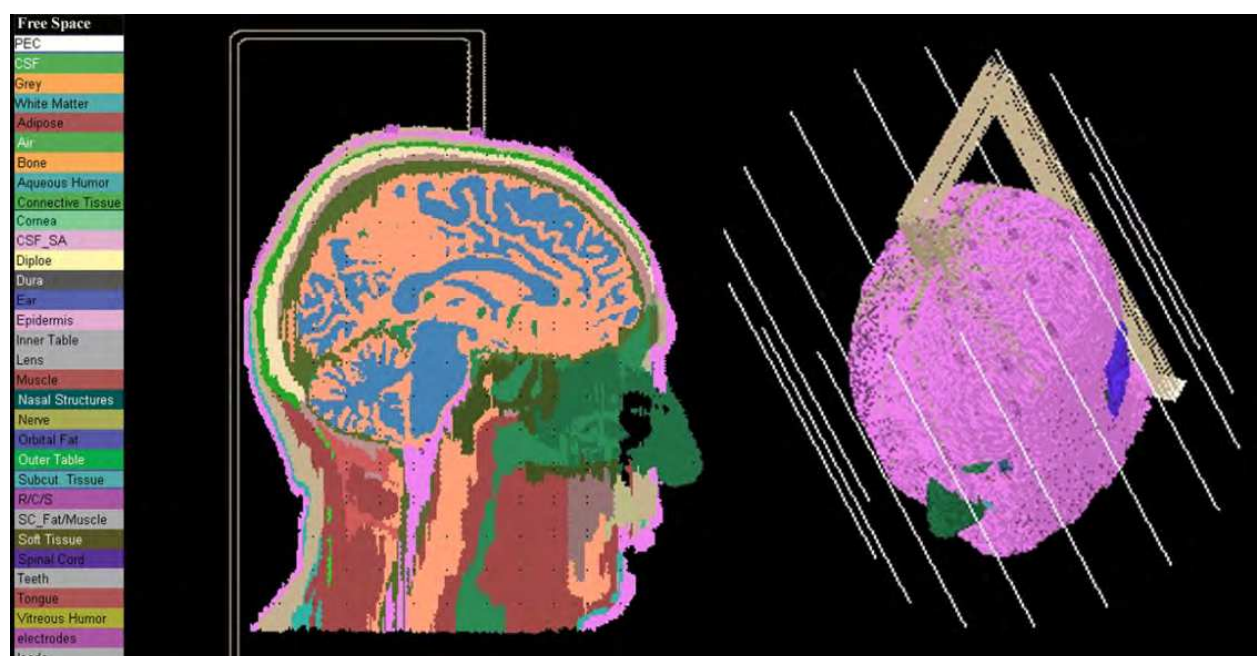

Fig. 1. High resolution head model with 32 electrodes/leads and RF coil. The 3D view shows the head model with EEG leads centered in a 16-wire RF coil.

Anatomical segmentation - Twenty-five non-brain anatomical structures (**Figure 1**) were manually segmented from the MRI data by an expert anatomist [Makris 2008]. Three brain structures (Cerebro Spinal Fluid, Grey and White matter) were additionally segmented with an automatic segmentation algorithm [Dale 1999, Segonne 2004] and coregistered with the non-brain structures. The final head model consisted of a total of 28 anatomical structures (**Table 1**). The total number of Yee cells [Yee 1966] was 4,642,730. The head dimensions were 170 mm in width, 217 mm in depth, and 238 mm in height.

	Anatomical Structures	Heterogeneous			Homogeneous		
		Density (kg/m³)	300 MHz [d]		Density (kg/m³)	300 MHz [d]	
			σ (S/m)	ε_r		σ (S/m)	ε_r
BRAIN	Grey Matter	1030(a)	0.69	60.00			
	White Matter	1030(a)	0.41	43.77			
	Cerebro Spinal Fluid	1010(a)	2.22	72.73			
NON-BRAIN	Adipose	920[a]	0.07	11.74	1040	0.80	59
	Air (Resp./Diges./Sinus)	1.3[b]	0.00	1.00			
	Bone (Facial)	1850[b]	0.08	13.43			
	Connective Tissue	1100[a]	0.55	46.77			
	Cornea	1076[c]	1.15	61.37			
	Diploe / Bone Marrow	1080[b]	0.21	23.16			
	Dura	1030[a]	0.80	47.95			
	Ear / Pinna	1100[a]	0.55	46.77			
	Eye Humor (Aqueous)	1010[a,c]	1.51	69.01			
	Eye Humor (Vitreous)	1010[a,c]	1.51	69.01			
	Eye Lens	1100[c]	0.64	48.95			
	Epidermis/Dermis	1100[a]	0.64	49.82			
	Inner Table	1850[b]	0.08	13.43			
	Muscle	1040[d]	0.79	58.97			
	Nasal-Structures	1100[a]	0.55	46.77			
	Nerve	1040[a]	0.41	36.90			
	Orbital Fat	920[a]	0.07	11.74			
	Outer Table	1850[b]	0.08	13.43			
	Retina/Choroid/Sclera	1170[a]	0.97	58.90			
	Spinal Cord	1040[a]	0.41	36.90			
	Soft Tissue	1100[a]	0.55	46.77			
	Subcutaneous Tissue	1100[a]	0.55	46.77			
	Subcutaneous Fat	920[a]	0.07	11.74			
	Teeth	1850[b]	0.08	13.43			
	Tongue	1040[d]	0.79	58.97			

Table 1. Anatomical structures and electrical properties of high-resolution heterogeneous head model at 300 MHz. The electrical properties were constant for all the anatomical structures in the homogeneous model. (a) [Li 2006]; (b) [Collins 2004], (c) [DeMarco 2003], (d) [FCC website] based on [Gabriel 1996].

Classification of anatomical structures at radio-frequency by their electrical properties - The classification of anatomical structures in terms of electrical properties is necessary to precisely compute the EM field and SAR in the human head during an MRI experiment. The electrical properties of anatomical structures, such as electrical conductivity and permittivity, vary depending on their structural composition. Specifically, the electrical

properties of the models used in this study were considered as [Vorst 2006]: a) linear with electric field, b) isotropic, c) dispersive, and d) heterogeneous in space. Under these conditions, complex permittivity (ε^*) is defined as:

$$\varepsilon^*(\omega) = \varepsilon_r(\omega) - j\varepsilon''(\omega)$$

$$= \varepsilon_r(\omega) - j\frac{\sigma_{tot}(\omega)}{\omega\varepsilon_0} = \varepsilon_r(\omega) - j\left(\frac{\sigma_i(\omega)}{\omega\varepsilon_0} + \varepsilon_d(\omega)\right) \tag{2}$$

where $\varepsilon_r(\omega)$ is the frequency-dependent relative permittivity of the material, ε_0 is the permittivity of free space (equal to $8.854 \cdot 10^{-12}$ F m^{-1}), ω is the angular frequency of the field ($\omega = 2\pi f$, with f frequency in Hz); $\varepsilon''(\omega)$ is the frequency-dependent loss factor, with $\sigma_{tot}(\omega)$ the total conductivity, that includes a frequency-independent ionic conductivity ($\sigma_i(\omega)$) and the frequency-dependent losses due to dielectric polarization ($\varepsilon_d(\omega)$). The frequency used in this study was 300 MHz which is approximately the RF frequency needed to elicit proton MRI signal at 7 T.

In the EEG leads, typically built with metals or non-biological materials, the loss component is due to free electrons only:

$$\varepsilon''(\omega) = \frac{\sigma_{tot}(\omega)}{\omega\varepsilon_0} = \frac{\sigma_i(\omega)}{\omega\varepsilon_0} \tag{3}$$
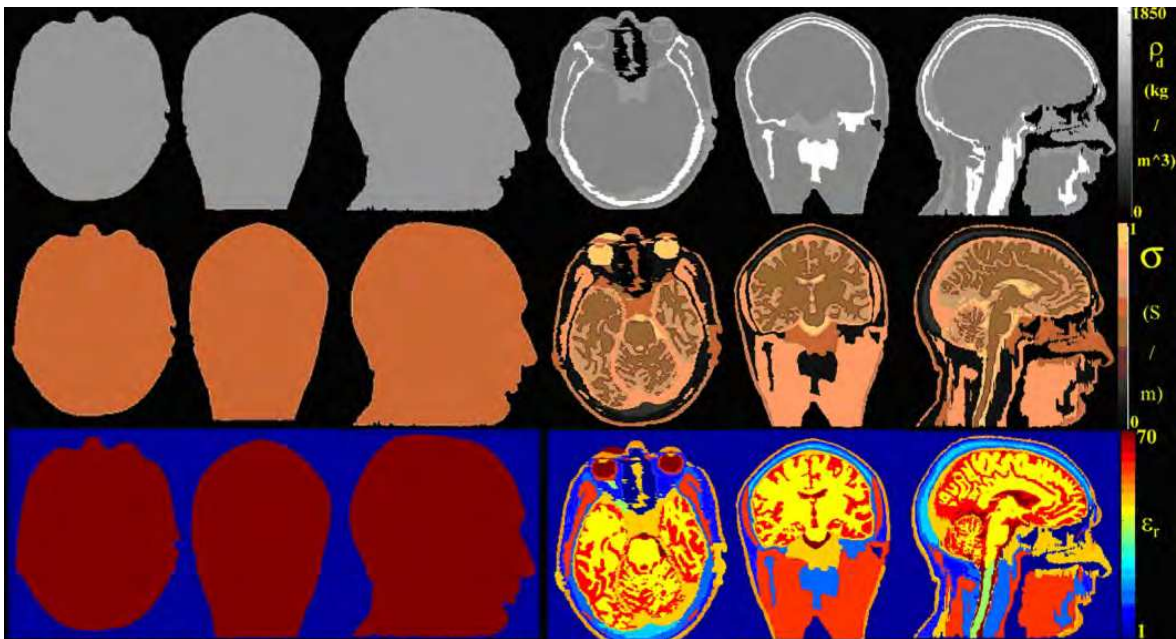

Fig. 2. Biophysical properties for homogeneous and heterogeneous model at 300 MHz. The high-spatial resolution of the model allowed distinguishing contiguous structures with different electrical properties, such as bone-marrow vs. outer table, skin vs. fat.

The anatomical classification, mass density and electrical properties at 300 MHz are shown in **Table 1** and mapped in **Figure 2**. Two different electrical models - a homogeneous and a heterogeneous one - were implemented. For the homogeneous case, the same physical

properties were assigned to all the anatomical structures, i.e., conductivity $\sigma_{tot} = 0.8 \, \text{S/m}$, relative permittivity $\varepsilon_r = 59$, and density $\rho_d = 1040 \, \text{kg/m}^3$, corresponding to the average properties of muscle at 300 MHz [FCC Website]. For the heterogeneous model, each anatomical structure was assigned more specific electrical properties, based on the data of the comprehensive study by Gabriel et al. [Gabriel 1996a, 1996b, 1996c] (**Table 1**). The values of mass density were derived from literature [Collins 2004, DeMarco 2003, Gabriel 1996, FCC website, Li 2006]. An average value of conductivity and permittivity was assigned to the anatomical structures without a direct equivalence in the database (i.e., "Subcutaneous Tissue", "Connective Tissue", and "Soft tissue") [Makris 2008].

Numerical Model of EEG electrodes and Leads - The layout of thirty-two EEG electrodes on a 2D mask was designed using Circuit Maker (Altium Inc, San Diego, CA) and imported into Matlab (Mathworks, Natick, MA). The mask was co-registered with the axial slice of largest diameter on the head model. The EEG electrodes and leads of the mask were projected and placed on the surface of the head model ("epidermis" tissue, see **Figure 1**) [Angelone 2006]. The EEG electrodes were modeled as small cylinders (radius: 7 mm, thickness: 3 mm) and were positioned in direct contact with the skin as for the expanded 10-20 montage [Regan 1989]. The leads were modeled as metallic leads ($\rho_{el/leads} = \rho_{copper} = 1.67 \cdot 10^{-8} \, \Omega \, m$), and were bundled above the Cz electrode [Regan 1989], oriented vertically, and curved downward as shown in **Figure 1**. The complete model (i.e., head with 32 EEG electrodes/leads) was then imported into the XFDTD software (Remcomi Inc., State College, PA). EEG leads were shortened on one side, to simulate the short circuit created by the low-pass filter in the input stage of the EEG recording system [Purdon 2008], and connected on the other side to the head surface.

Numerical Model of RF Coil - The RF source was based on a volume RF coil [Jin 1997, Collins 2001]. The coil was modeled with 16 perfect electrically conductive rods of 295 mm in length and disposed around the head with circular symmetry (diameter 260mm) (**Figure 1**). The RF source was simulated as a circular excitation driving the current generators placed on the centers of the rods with 1A peak-to-peak amplitude and a 22.5° phase-shift between any two adjacent generators.

FDTD simulations - Numerical simulations were performed using commercially available software XFDTD, based on the Finite-Difference-Time-Domain (FDTD) algorithm. Numerical simulations were performed at a frequency of 300 MHz. A total of seven perfectly matching layers were used for boundary conditions [Berenger 1994]. The total volume, including the free space around the model, was 297×353×303 mm³; the time step used to meet the Courant condition for numerical stability [Taflove 2005] was 1.92 ps, and the total number of time steps was 25,000. Simulations provided the magnitude of electromagnetic field and induced currents for each voxel, as well as whole-head averaged SAR, 1g- and 10 g-averaged SAR [IEC 2002, FDA 2003].

3. Results

Model without EEG electrodes/leads - **Figure 3** shows the magnetic flux density $\|\vec{B}\|$, and **Figure 4** the electric field $\|\vec{E}\|$ and induced currents $\|\vec{J}\|$ computed with homogeneous and heterogeneous head model. The load of the head on the RF coil (i.e. the impedance seen by each of the 16 sources) was similar (± 10%) in both models, in line with physical RF coil

tuning on the bench with anatomically accurate phantoms or human head [Ibrahim 2005]. The characteristic Central Brightening Effect at 7T [Collins 2005] was present in both models. The superposition of electromagnetic fields determined a complex pattern of electric field inside the head and local peaks of electric field at the boundaries between skin and air as well as inside the head. The effect of the tissue conductivity focused the currents in the most conductive structures (e.g., Cerebro Spinal Fluid and eye region).
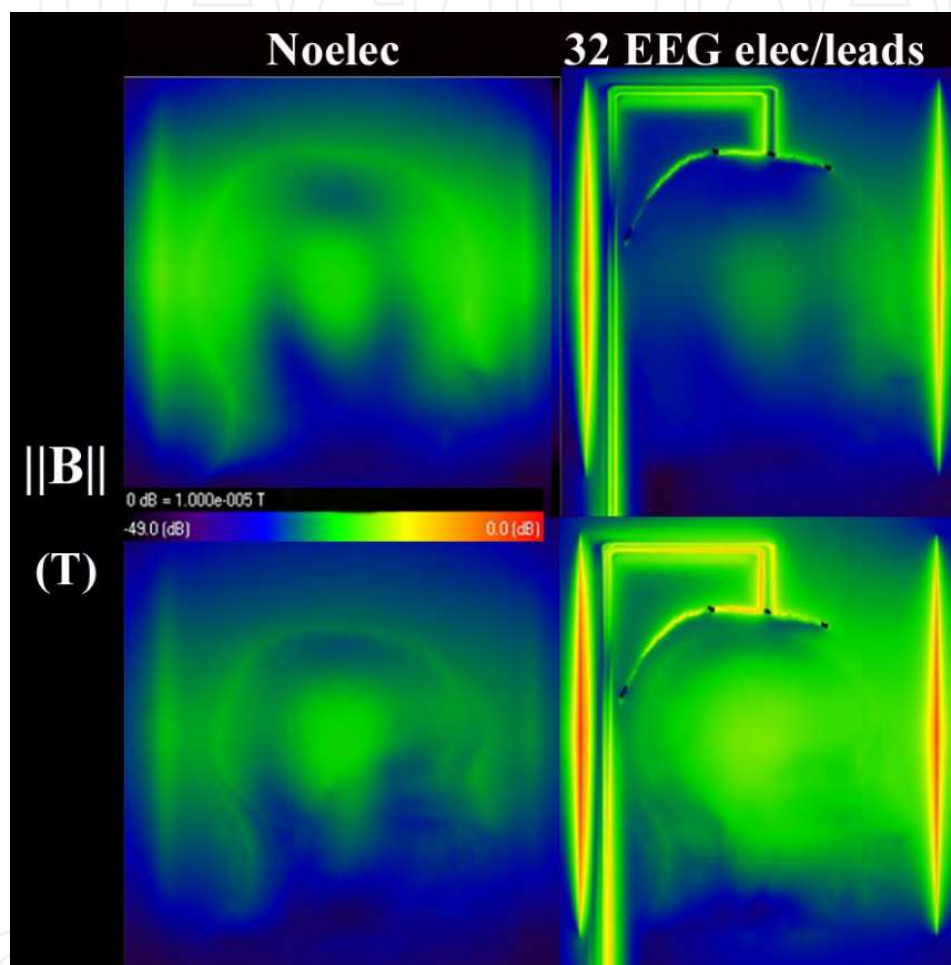
Fig. 3. Amplitude of magnetic flux density $\left\| \vec{B} \right\|$ computed with homogeneous and heterogeneous head model without ("Noelec") and with EEG electrodes/leads. The characteristic Central Brightening Effect at 7T [Collins 2005] was present in both models.

Head plus metallic leads - **Figure 4** shows the effect of metallic leads with the head. The superposition of the electric field radiated from the RF coil and field scattered by the leads resulted in an increase of the field near the leads and on the skin, and in a reduction of the field at the center of the head ("shielding effect of the EEG leads") [Hamblin 2007]. There was a peak of induced currents on the skin, near the leads. Because of the EEG-leads acting as antennas, the coil load and the magnetic field inside the head were different compared to the control case of no leads.
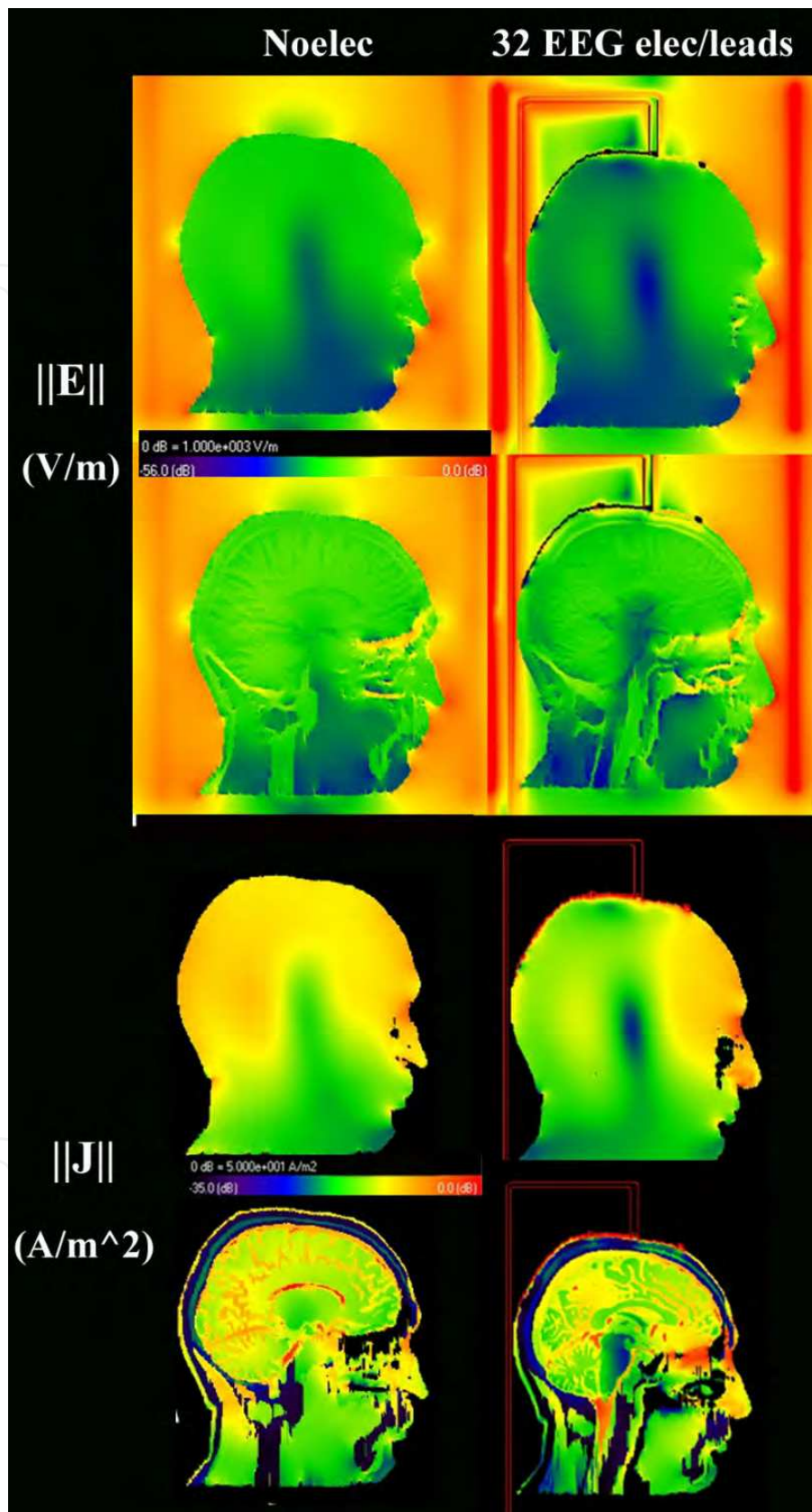
Fig. 4. Amplitude of electric field $\left\|\vec{E}\right\|$ and induced currents $\left\|\vec{J}\right\|$ computed with homogeneous and heterogeneous head model, without ("Noelec") and with EEG electrodes/leads.

SAR - The whole-head SAR computed with the two models (with/without leads) was similar (i.e., 3% difference, see **Table 2**). No significant difference (<5%) in whole-head SAR was observed for the case with perfectly conductive EEG leads. The heterogeneity of the structures and the local differences of electrical properties affected the 1g-averaged SAR, with up to two-fold difference for the peak 1g-averaged SAR (**Figure 5**) in the control case without leads (1st vs. 3rd column, **Table 2**), and a 30% difference with EEG leads (2nd vs. 4th column, **Table 2**). Smaller differences with homogeneous vs. heterogeneous model were observed in the computation of 10-g averaged SAR, with a 15% difference without leads and 20% difference with EEG leads (**Table 2**).

300 MHz	Homogeneous		Heterogeneus	
	noelec	32elec-copper	noelec	32elec-copper
Max SAR [W/kg]	1.1	33.9	2.3	38.8
Peak 1g avg. SAR [W/kg]	0.48	1.37	0.92	1.05
Peak 10g avg. SAR [W/kg]	0.29	0.32	0.33	0.40
Whole Head [W/kg]	0.10	0.09	0.10	0.09
Input power [W]	4.1	3.3	4.5	3.6
Power dissipated in head[W]	2.0	1.4	2.4	1.8
Radiated power [W]	2.1	1.8	2.1	1.9
Efficiency	52%	56%	47%	51%

Table 2. Results for simulations with homogeneous and heterogeneous model, without and with copper EEG leads.

4. Discussion

While the results in the homogeneous model can be validated with direct measurements in phantoms, the validation of numerical simulations with heterogeneous head models require a multi-structure phantom, which would be much more cumbersome and expensive to build. This study aimed to evaluate whether the use of a more complex heterogeneous model would provide additional information when looking at SAR changes due to EEG electrodes/leads in a human head exposed to a 300 MHz RF field.

For this purpose, the study was based on a high-resolution head model segmented by an expert anatomist from MRI data of an adult healthy subject (**Figure 1**). In the control-case of a head model without EEG electrodes/leads, thei EM field was slightly asymmetric [Amjas 2005, Sled 1998]. The EM fields and induced currents were also different between the homogeneous and heterogeneous models [Amjad 2005].
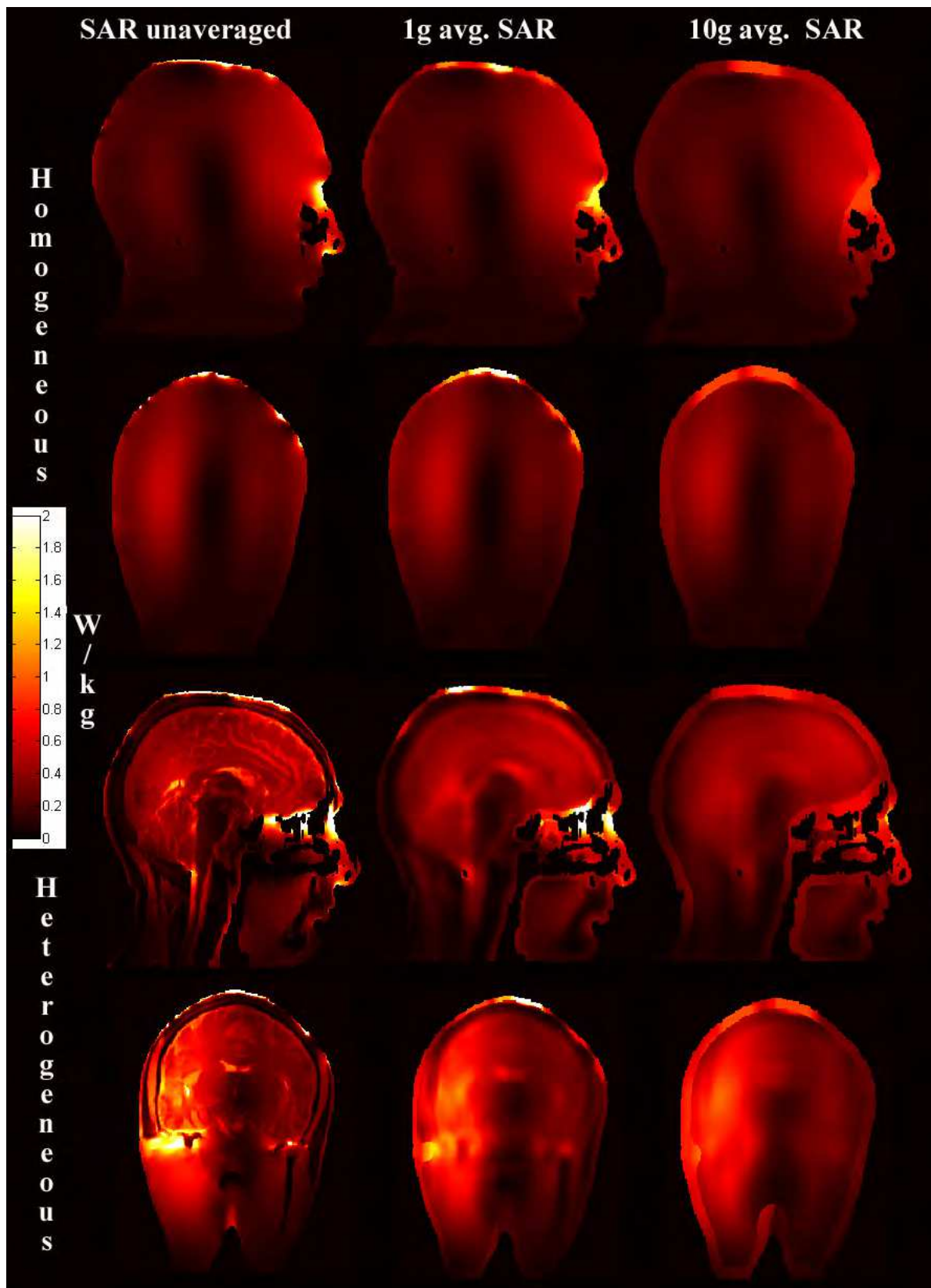
Fig. 5. Specific Absorption Rate (SAR) computed with an electrically homogeneous (top) and electrically heterogeneous (bottom head) model. Sagittal and coronal maps for SAR unaveraged, 1g-averaged and 10g-averaged SAR are shown.
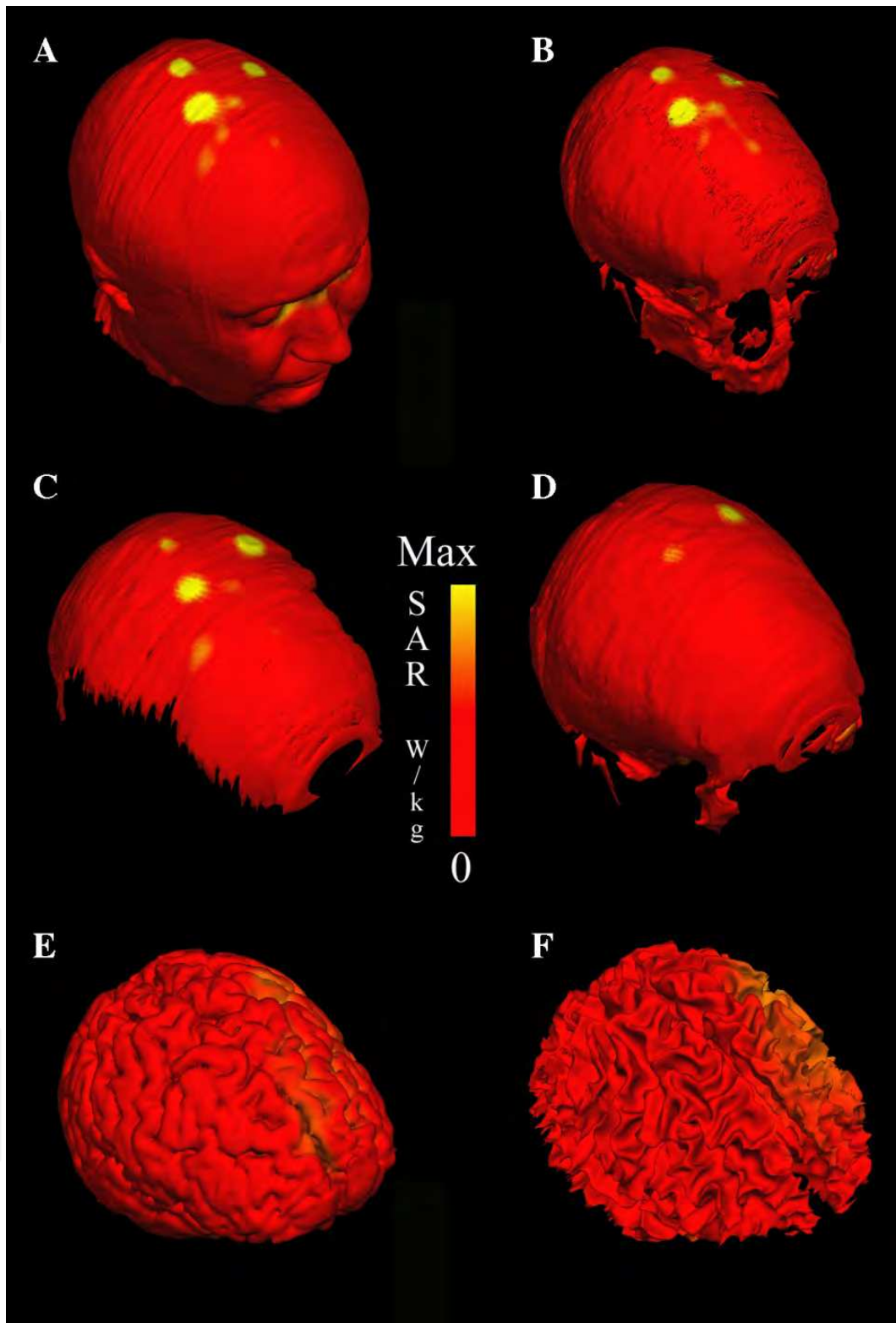
Fig. 6. 3D view of SAR (W/Kg) with copper leads on epidermis and bone structures
(outer table, inner table, bone, teeth). The high-resolution of the model allowed for precise
anatomical definition of thin structures, such the epidermis, where the contact with copper
EEG leads induces local electric field and SAR enhancement. Max SAR = 10 W/kg.
Values normalized to 1 W of Input Power.

SAR estimation with homogeneous and heterogeneous model- No significant differences were observed for whole-head SAR computed with or without EEG leads for both the homogeneous and heterogeneous models, suggesting that whole-head SAR may be an excessively smoothing parameter for RF dosimetry with EEG leads. The small difference in peak SAR estimated with homogeneous or heterogeneous model for the case with metallic EEG leads was likely due to the specific location of the peak SAR (i.e., few mm underneath the electrodes); the volume of interest in the heterogeneous model included only two structures, epidermis and subcutaneous tissue, with electrical properties similar to the one used for the homogeneous model. On the other hand, because of the spatially-limited characteristics of SAR changes it is important to properly model the variably-conductive interfaces between EEG electrodes, epidermis, and subcutaneous tissues, both in terms of anatomical structures and electrical properties. As a further test, we have compared the results obtained with the homogeneous model with metallic leads with a model where the external layer (i.e., the epidermis) was substituted with perfectly insulating material ($\sigma = 0\ S/m$). Whole-head and 10g-averaged SAR were not affected by the dramatic change in conductivity at the interface, but there was a 280% change in computed 1g-averaged SAR.

The use of a heterogeneous head model may allow for improved SAR computation and visualization for heterogeneous structures with different electrical properties, such as skin, fat, muscle or bone marrow (**Figure 2**). However, the use of an anatomically fine-grained head model may add potential errors when modeling the internal structures of the head [Gajsek 2002]. Due to the difficulties in matching exactly all the anatomical definitions to existing literature, some of the anatomical structures were assigned the same electrical properties; 16 different electrical properties were used to characterize the anatomical structures (**Figure 2**). Further work may be performed to improve the electrical characterization of the numerical head model and to validate using direct measurements with corresponding physical models.

Effect of geometry - This study focused on evaluating the effect of head electrical heterogeneity as well as lead resistivity on SAR. The geometrical model was constant with respect to other physical variables (**Figure 1**) which may affect SAR: number of electrodes, length and orientation of the leads, position of the head inside the RF coil, and RF source geometry, as well as size and shape of the head model. In clinical applications, these variables will be affected by various external constraints, such as length of the imager used for the MRI recording, position of EEG system inside the MRI room, and geometry of RF coil used to obtain the best Signal to Noise Ratio (SNR). For example, EEG leads may be connected to a pre-amplifier placed either on the back of the imager (EEG leads from the top of the head oriented farther away from the head) or in the front of the scanner (EEG leads placed along the head and exiting from the neck down); in this case the minimal physical length of the leads will depend on the placement of the pre-amplifier. We have modeled 32 electrodes and leads, a configuration currently used in many laboratories for EEG-MRI recordings. The results of this study cannot be directly extrapolated to different number of electrodes, because the presence of more leads may increase the interaction with the EM field, with resulting SAR in the head that could be higher or lower, depending on the geometry, the shielding effect of the EEG leads [Hamblin 2007] and the frequency considered [Angelone 2004].

Antenna effect - The typical length of EEG leads is in the order of ~ 50-100cm, which is comparable with the wavelength of the RF field at 300 MHz (i.e., 1 m in empty space). The interactions of the EEG leads and RF coils will induce changes in the EM field inside the head (i.e., "shielding effect" of the EEG leads) [Hamblin 2007] and local SAR enhancement at the interface between electrodes and skin [Armenean 2004, Yeung 2002]. Low resistivity EEG leads ($\rho_{lead} < \rho_{min} \approx 0.0001\,\Omega\,m$) behave as lossless antenna [Balanis 2005] and will have maximum induced currents along the leads. The high discontinuity of resistivity between lead and surrounding medium ($\rho_{lead} = 1.67 \cdot 10^{-8}\Omega\,m$ vs. $\rho_{skin} = 1/\sigma_{skin}\,1.56\,\Omega\,m$ for the skin/epidermis, **Table 1**) determines an electric field enhancement at the interface between leads and head surface (i.e., epidermis). This observation is in line with theoretical models [Guy 1975] and physical evidence of reports of burns due to "antenna-effect" of leads [Dempsey 2001].

5. Conclusions

The aim of this study was to investigate the possible effect of using complex heterogeneous head models when investigating SAR in a human head wearing EEG electrodes/leads while exposed to RF field of high-field MRI. MRI-based high-resolution homogeneous and heterogeneous head models with 32 EEG electrodes/leads were implemented. Electromagnetic simulations based on FDTD algorithm were performed. Non-significant differences in whole-head SAR (i.e. less than 5%) and a 30% difference in peak 10g-averaged SAR values were observed with the homogeneous vs. heterogeneous models. The presence of an insulating layer between EEG electrode and skin resulted in a three-fold change in computed 1g-averaged SAR. Results of this study suggest that when whole-head, 10g-averaged, and 1g-averaged SAR in a human head wearing EEG electrodes/leads are computed with a homogeneous rather than electrically heterogeneous model this can result in a difference of up to 30%. In all cases, a precise modeling of the electrically conductive interface between electrode and head surface is fundamental to avoid a significant underestimation of the local SAR.

Future directions – The systematic analysis presented in this chapter improved the scientific understanding of the complex interactions between radiofrequency electromagnetic field and a human head with EEG leads. Such a numerical framework can be used to support the design and development of novel leads for multimodal recording at ultra high-field MRI. Future work may be directed toward investigating the effect of the specific head model used, in terms of inter-subject variability and in the presence of anatomical pathologies. Moreover, further improvement of the electrical model, namely the electrical properties associated with each anatomical structure, can be obtained by taking advantage of MRI-based direct measurements, i.e., electrical properties tomography (EPT). Finally, while the specific absorption rate is the current parameter used for RF dosimetry, the use of temperature is a more biologically significant quantity, and future work may be directed toward a better evaluation of the changes in temperature – rather than only SAR – in the body. The experimental validation with properly matching geometries between numerical and physical models will most likely be the final fundamental step toward a complete dosimetric evaluation.

6. Acknowledgments

7. References

Adair E.R., and Berglund L.G. On the thermoregulatory consequences of NMR imaging. Magn Reson Imaging, 1986. 4(4): p. 321-33.

Allen P.J., Josephs O., and Turner R. A method for removing imaging artifact from continuous EEG recorded during functional MRI. Neuroimage, 2000. 12(2): p. 230-9.

Amjad A., Kamondetdacha R., Kildishev A., Park S.M., and Nyenhuis J. Power deposition inside a phantom for testing of MRI heating. IEEE Trans on Magnetics, 2005. 41(10): p. 4185-4187.

Angelone L.M., Potthast A., Segonne F., Iwaki S., Belliveau J., and Bonmassar G. Metallic electrodes and leads in simultaneous EEG-MRI: specific absorption rate (SAR) simulation studies. Bioelectromagnetics, 2004. 25(4): p. 285-295.

Angelone L.M., Vasios C.E., Wiggins G., Purdon P.L., and Bonmassar G. On the effect of resistive EEG electrodes and leads during 7 T MRI: simulation and temperature measurement studies. Magn Reson Imaging, 2006. 24(6): p. 801-12

Armenean C., Perrin E., Armenean M., Beuf O., Pilleul F., and Saint-Jalmes H. RF-induced temperature elevation along metallic wires in clinical magnetic resonance imaging: influence of diameter and length. Magn Reson Med, 2004. 52(5): p. 1200-6.

Balanis, C.A., Antenna theory : analysis and design. 3rd ed. 2005, Hoboken, NJ: John Wiley. xvii, 1117 p.

Benar C., Aghakhani Y., Wang Y., Izenberg A., Al-Asmi A., Dubeau F., and Gotman J. Quality of EEG in simultaneous EEG-fMRI for epilepsy. Clin Neurophysiol, 2003. 114(3): p. 569-80.

Berenger J.P. A perfectly matched layer for the absorption of electromagnetic waves. Computational Physics, 1994. 114: p. 185-200.

Bonmassar G., Hadjikhani N., Ives J.R., Hinton D., and Belliveau J.W. Influence of EEG electrodes on the BOLD fMRI signal. Hum Brain Mapp, 2001. 14(2): p. 108-15.

Bottomley P.A. and Andrew E.R. RF magnetic field penetration, phase shift and power dissipation in biological tissue: Implications for NMR imaging. Phys. Med. Biol., 1978. 23: p. 630–643.

Collins C.M., and Smith M.B. Spatial resolution of numerical models of man and calculated specific absorption rate using the FDTD method: a study at 64 MHz in a magnetic resonance imaging coil. J Magn Reson Imaging, 2003. 18(3): p. 383-8.

Collins C.M., Liu W., Wang J., Gruetter R., Vaughan J.T., Ugurbil K., and Smith M.B. Temperature and SAR calculations for a human head within volume and surface coils at 64 and 300 MHz. J Magn Reson Imaging, 2004. 19(5): p. 650-6.

Collins C.M., Liu W., Schreiber W., Yang Q.X., and Smith M.B., Central brightening due to constructive interference with, without, and despite dielectric resonance. J Magn Reson Imaging, 2005. 21(2): p. 192-6.

Comi E., Annovazzi P., Silva A.M., Cursi M., Blasi V., Cadioli M., Inuggi A., Falini A., Comi G., and Leocani L. Visual evoked potentials may be recorded simultaneously with fMRI scanning: A validation study. Hum Brain Mapp, 2005. 24(4): p. 291-298.

Dale A.M., Fischl B., and Sereno M.I. Cortical surface-based analysis. I. Segmentation and surface reconstruction. Neuroimage, 1999. 9(2): p. 179-94.

DeMarco S.C., Lazzi G., Liu W., Weiland J.D., and Humayun M.S. Computed SAR and thermal elevation in a 0.25-mm 2-D model of the human eye and head in response to an implanted retinal stimulator - part I: models and methods. Antennas and Propagation, IEEE Transactions on, 2003. 51(9): p. 2274-2285.

Dempsey M.F., Condon B., and Hadley D.M. Investigation of the factors responsible for burns during MRI. J Magn Reson Imaging, 2001. 13(4): p. 627-31.

Federal Communication Commission http://www.fcc.gov/fcc-bin/dielec.sh

Food and Drug Administration (FDA) Center for Devices and Radiological Health. *Criteria for Significant Risk Investigations of Magnetic Resonance Diagnostic Devices*. 2003.

Gandhi O.P., and Chen X.B. Specific absorption rates and induced current densities for an anatomy-based model of the human for exposure to time-varying magnetic fields of MRI. Magn Reson Med, 1999. 41(4): p. 816-23.

Gabriel C., Gabriel S., and Corthout E. The dielectric properties of biological tissues: I. Literature survey. Phys. Med. Biol., 1996. 41: p. 2231–2249.

Gabriel C., Gabriel S., and Corthout E. The dielectric properties of biological tissues: II. Measurements in the frequency range 10 Hz to 20 GHz. Phys. Med. Biol., 1996. 41: p. 2251–2269.

Gabriel C., Gabriel S., and Corthout E. The dielectric properties of biological tissues: III. Parametric models for the dielectric spectrum of tissues. Phys. Med. Biol., 1996. 41: p. 2271–2293.

Gajsek P., Walters T.J., Hurt W.D., Ziriax J.M., Nelson D.A., and Mason P.A. Empirical validation of SAR values predicted by FDTD modeling. Bioelectromagnetics, 2002. 23(1): p. 37-48.

Goldman R.I., Stern J.M., Engel J. Jr., and Cohen M.S. Simultaneous EEG and fMRI of the alpha rhythm. Neuroreport, 2002. 13(18): p. 2487-92.

Guy A. W. Biophysics - Energy Absorption and Distribution, vol. AGARD Lectures Series 78, p. 4-1 to 4-14, 1974.

Hamblin D.L., Anderson V., McIntosh R.L., McKenzie R.J., Wood A.W., Iskra S., and Croft R.J. EEG electrode caps can reduce SAR induced in the head by GSM900 mobile phones. IEEE Trans Biomed Eng, 2007. 54(5): p. 914-920.

Iannetti G.D., Niazy R.K., Wise R.G., Jezzard P., Brooks J.C., Zambreanu L., Vennart W., Matthews P.M., and Tracey I. Simultaneous recording of laser-evoked brain potentials and continuous, high-field functional magnetic resonance imaging in humans. Neuroimage, 2005. 28(3): p. 708-19.

Ibrahim T.S., Kangarlu A., and Chakeress D.W. Design and performance issues of RF coils utilized in ultra high field MRI: experimental and numerical evaluations. IEEE Trans Biomed Eng, 2005. 52(7): p. 1278-84.

Ibrahim T.S., Mitchell C., Abraham R., and Schmalbrock P. In-depth study of the electromagnetics of ultrahigh-field MRI. NMR Biomed, 2007. 20(1): p. 58-68.

IEC, International Standard, medical equipment - part 2-33: Particular requirements for the safety of the magnetic resonance equipment for medical diagnosis, 2nd revision. 2002, International Electrotechnical Commission 601-2-33: Geneva. p. 29-31.

Jin J., and Chen J. On the SAR and field inhomogeneity of birdcage coils loaded with the human head. Magn Reson Med, 1997. 38(6): p. 953-63.

Kainz W., Chan D.D., Casamento J.P., and Bassen H.I. Calculation of induced current densities and specific absorption rates (SAR) for pregnant women exposed to hand-held metal detectors. Phys Med Biol, 2003. 48(15): p. 2551-60.

Kobayashi, E., Bagshaw A.P., Jansen A., Andermann F., Andermann E., Gotman J., and Dubeau F. Intrinsic epileptogenicity in polymicrogyric cortex suggested by EEG-fMRI BOLD responses. Neurology, 2005. 64(7): p. 1263-6.

Kunz K.S., and Luebbers R.J. The finite difference time domain method for electromagnetics. 1993, Boca Raton: CRC Press. 448 p.

Lemieux L., Allen P.J., Franconi F., Symms M.R., and Fish D.R. Recording of EEG during fMRI experiments: patient safety. Magn Reson Med, 1997. 38(6): p. 943-52.

Li Q.X., and Gandhi O.P. Thermal Implications of the New Relaxed IEEE RF Safety Standard for Head Exposures to Cellular Telephones at 835 and 1900 MHz. IEEE Trans Microwave Theory and Technique, 2006. 54(7): p. 3146-3154.

Liebenthal E., Ellingson M.L., Spanaki M.V., Prieto T.E., Ropella K.M., and Binder J.R. Simultaneous ERP and fMRI of the auditory cortex in a passive oddball paradigm. Neuroimage, 2003. 19(4): p. 1395-404.

Makris N, Angelone L, Tulloch S, Sorg S, Kaiser J, Kennedy D, Bonmassar G. MRI-based anatomical model of the human head for specific absorption rate mapping. Med Biol Eng Comput. 2008. 46(12): p. 1239-1251.

Matsuda T., Matsuura M., Ohkubo T., Ohkubo H., Atsumi Y., Tamaki M., Takahashi K., Matsushima E., and Kojima T. Influence of arousal level for functional magnetic resonance imaging (fMRI) study: simultaneous recording of fMRI and electroencephalogram. Psychiatry Clin Neurosci, 2002. 56(3): p. 289-90.

Mirsattari S.M., Lee D.H., Jones D., Bihari F., and Ives J.R. MRI compatible EEG electrode system for routine use in the epilepsy monitoring unit and intensive care unit. Clin Neurophysiol, 2004. 115(9): p. 2175-80.

Mulert C., Jager L., Propp S., Karch S., Stormann S., Pogarell O., Moller H.J., Juckel G., and Hegerl U. Sound level dependence of the primary auditory cortex: Simultaneous measurement with 61-channel EEG and fMRI. Neuroimage, 2005. 28(1): p. 49-58.

Mullinger K., Debener S., Coxon R., and Bowtell R. Effects of simultaneous EEG recording on MRI data quality at 1.5, 3 and 7 Tesla. Int J Psychophysiol. 2008 Mar;67(3): p. 178-88.

National Council Radiation Protection and Measurements (NCRP). Radiofrequency electromagnetic fields: properties, quantities and units, biophysical interaction, and measurement. 1981, Bethesda, MD.

Nitz W.R., Brinker G., Diehl D., and Frese G. Specific absorption rate as a poor indicator of magnetic resonance-related implant heating. Invest Radiol, 2005. 40(12): p. 773-6.

Polk C. and Postow E. CRC handbook of biological effects of electromagnetic fields. 1986, Boca Raton, Fla.: CRC Press. 503 p.

Purdon PL, Millan H, Fuller PL, Bonmassar G. An open-source hardware and software system for acquisition and real-time processing of electrophysiology during high field MRI. J Neurosci Methods. 2008 Nov 15;175(2): p.165-86.

Purdon PL, Pierce ET, Bonmassar G, Walsh J, Harrell PG, Kwo J, Deschler D, Barlow M, Merhar RC, Lamus C, Mullaly CM, Sullivan M, Maginnis S, Skoniecki D, Higgins HA, Brown EN. Simultaneous electroencephalography and functional magnetic resonance imaging of general anesthesia. Ann N Y Acad Sci. 2009 Mar;1157: p.61-70.

Regan D. Human brain electrophysiology: Evoked potentials and evoked magnetic fields in science and medicine. 1989, New York: Elsevier, 415 p.

Scarff C.J., Reynolds A., Goodyear B.G., Ponton C.W., Dort J.C., and Eggermont J.J. Simultaneous 3-T fMRI and high-density recording of human auditory evoked potentials. Neuroimage, 2004. 23(3): p. 1129-42.

Schenck J. Safety of strong, static magnetic fields. J Magn Reson Imaging, 2000. 12(1): p. 2-19.

Segonne F., Dale A.M., Busa E., Glessner M., Salat D., Hahn H.K., and Fischl B. A hybrid approach to the skull stripping problem in MRI. Neuroimage. 2004 Jul; 22(3): p. 1060-75.

Shellock F.G. Reference Manual for Magnetic Resonance Safety, Implants, and Devices: 2011. Biomedical Research Publishing Company, 650 p.

Sled J. G., and Pike G. B. Standing-wave and RF penetration artifacts caused by elliptic geometry: an electrodynamic analysis of MRI.1998, IEEE Trans. Med. Imaging, vol. 17, p. 653-662

Stern J.M., Simultaneous electroencephalography and functional magnetic resonance imaging applied to epilepsy. Epilepsy Behav, 2006. 8(4): p. 683-92.

Taflove A., and Hagness S. C. Computational Electrodynamics: The Finite-Difference Time-Domain Method, 3rd ed. 2005, Artech House, Norwood, MA.

Trakic, A., F. Liu, H.S. Lopez, H. Wang, and S. Crozier, Longitudinal gradient coil optimization in the presence of transient eddy currents. Magn Reson Med, 2007. 57(6): p. 1119-30.

Van den Berg C.A., van den Bergen B., Van de Kamer J.B., Raaymakers B.W., Kroeze H., Bartels L.W., and Lagendijk J.J. Simultaneous B1 + homogenization and specific absorption rate hotspot suppression using a magnetic resonance phased array transmit coil. Magn Reson Med, 2007. 57(3): p. 577-86.

Vasios C.E., Angelone L.M., Purdon P.L., Ahveninen J., Belliveau J.W., and Bonmassar G. EEG/(f)MRI measurements at 7 Tesla using a new EEG cap ("InkCap"). Neuroimage, 2006. 33(4): p. 1082-92.

Vorst A.v., Rosen A., and Kotsuka Y. RF/microwave interaction with biological tissues. 2006, John Wiley & Sons, IEEE, Hoboken, N.J.: xiii, 330 p.

Yee K.S. Numerical Solution of Initial Boundary Value Problems Involving Maxwell's Equations in Isotropic Media. IEEE Transactions on Antennas and Propagation, 1966. 14(3): p. 302-307.

Yeung C.J., Susil R.C., and Atalar E. RF heating due to conductive wires during MRI depends on the phase distribution of the transmit field. Magn Reson Med, 2002. 48(6): p. 1096-8.
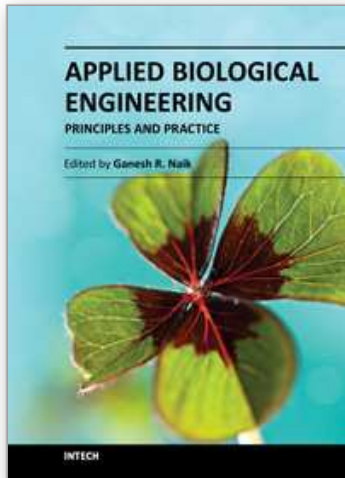
Applied Biological Engineering - Principles and Practice
Edited by Dr. Ganesh R. Naik

Biological engineering is a field of engineering in which the emphasis is on life and life-sustaining systems. Biological engineering is an emerging discipline that encompasses engineering theory and practice connected to and derived from the science of biology. The most important trend in biological engineering is the dynamic range of scales at which biotechnology is now able to integrate with biological processes. An explosion in micro/nanoscale technology is allowing the manufacture of nanoparticles for drug delivery into cells, miniaturized implantable microsensors for medical diagnostics, and micro-engineered robots for on-board tissue repairs. This book aims to provide an updated overview of the recent developments in biological engineering from diverse aspects and various applications in clinical and experimental research.

How to reference
In order to correctly reference this scholarly work, feel free to copy and paste the following:

Leonardo M. Angelone and Giorgio Bonmassar (2012). Specific Absorption Rate Analysis of Heterogeneous Head Models with EEG Electrodes/Leads at 7T MRI, Applied Biological Engineering - Principles and Practice, Dr. Ganesh R. Naik (Ed.), ISBN: 978-953-51-0412-4, InTech, Available from:
http://www.intechopen.com/books/applied-biological-engineering-principles-and-practice/specific-absorption-rate-analysis-of-heterogeneous-head-models-with-eeg-and-7t-mri-

INTECH
open science | open minds